ANODE DUSTING IN HALL - HEROULT CELLS

T. Foosnæs*, T. Naterstad*, M. Bruheim**, K. Grjotheim**

* R&D Carbon, ASV, N-5875 Ardalstangen, Norway
** University of Oslo, 0315 Oslo 3, Norway

A B S T R A C T

Operational irregularities originating from excessive dusting by selective anode oxidation have been experienced by most aluminum producers, particularly in Soderberg pots.

The spatial distribution of carbon particles in the bath of aluminum reduction cells has been characterized by a combination of optical microscopy and gravimetric oxidation methods. Samples covering the entire bath depth were obtained from prebaked and Soderberg cells by a specially designed sample collector, which was opened and closed while immersed in the melt. Quenched bath cores were sliced and prepared for microscopic gravimetric oxidation analysis to determine particle size distribution and total carbon content <u>versus</u> bath depth.

The oxidation rate of carbon in the bath was studied in separate bench scale experiments.

Results are discussed in terms of practical operational impacts and applications.

1. INTRODUCTION

Dusting in aluminum reduction pots is one of the visual signs of unwanted anode consumption. Before adressing the dusting phenomenon, a review of the main anode consumption mechanisms is helpful.

Anodes in aluminum reduction pots are consumed by electrochemical, chemical and mechanical processes (1,2). The major anode consumption (80 % of the theoretical (2)) is accounted for by the electrolytic process itself, through the equations

$$Al_2O_3 + 3/2C = 3/2CO_2 + 2Al \quad (1)$$
$$Al_2O_3 + 3C \ \ = 3CO + 2Al \quad (2)$$
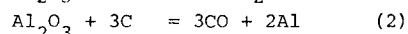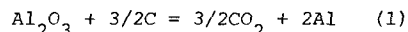
If carbon dioxide is the primary gas product by the electrolysis, i.e., the process is described by Eqn.(1) only, the theoretical carbon consumption is 334 kgC/tAl at 100 % current efficiency. The actual carbon consumption during aluminum electrolysis ranges from 420 to 550 kgC/tAl, and the excess consumption is due to the processes mentioned initially. The anode consumption decreases with increasing current density (4-6), due to a reduced reactive surface area.

Between 4 and 17 % of the anode is consumed through oxidation by air (3,7,8),

$$C + O_2 = CO_2 \quad (3)$$
$$2C + O_2 = 2CO \quad (4)$$

These reactions occur at the air - exposed parts of a prebaked anode (sides and top). Small concentrations of alkali or transition metal impurities in the carbon material catalyze the anode oxidation and contribute to an increased anode consumption (9-11), depending on the chemical form and distribution of the catalytic elements (12).

The second chemical anode consumption reaction is oxidation of the carbon material by CO_2. The

reaction occurs in the pores of the anode, immediately behind the electrode surface.

$$C + CO_2 = 2CO \qquad\qquad (5)$$

The rate of reaction (5) increases exponentially with temperature, and is approximately doubled by a temperature rise of 15 $^{\circ}$C in the temperature range 950 - 1000 $^{\circ}$C. Formation of CO inhibits the reaction between C and CO_2, thus the carbon dioxide reactivity decreases with decreasing current density (7,13).

Studies have shown that the surface area accessible for reaction (5) to a large extent is determined by the properties of the pitch coke (2,14,15). For prebaked anodes, this area varies with the anode baking temperature. For Soderberg anodes, the reaction accessible surface depends on the amount of pitch used, as well as the interaction between pitch and the carbon aggregate.

The balance between the carbon dioxide and air reactivity of the different carbon phases present in the anode is the key to the dusting phenomenon. As the pitch coke tends to be the most reactive phase of the carbon composite, selective oxidation erodes the material and causes carbon particles to loosen from the matrix and to accumulate in the bath. The transfer of carbon particles to the bath is facilitated by convection in the electrolyte (mechanical abrasion). Convection is caused by the continous release of anodic gas products, thermal gradients and the movement of the metallic pad in the magnetic field. Convection also contributes to vertical transport of carbon particles in the cell and may cause local enrichment of carbon particles under the anodes, which results in uneven wear of the electrolytic surface and thereby operational irregularities. Besides dusting due to selective oxidation, the migration of hydrocarbons from the binder phase through the cracks and pores of the anode may substantiate the dusting problem in Soderberg cells.

In the electric field of an aluminum reduction cell the carbon particle surfaces are polarized and the dust particles therefore act as electrical insulators, causing higher bath resistance. The effect of the increased cell resistance is a raise in the temperature of the electrolyte and of the anode. The anode consumption then increases due to the higher carbon dioxide - and oxygen reactivities of the anode (9,13) and more carbon dust is formed. Thus, a vicious circle with increasing operational problems is entered, which stresses the importance of using anodes with homogeneous reactivity with respect both to the CO_2 and the air oxidation.

2. EXPERIMENTAL

2.1 Sampling equipment and technique

For routine analyses, crucibles often are used to obtain samples for the electrolyte. The disadvantages with this sampling technique are that small samples are obtained near the bath surface, the samples will contain comparatively large amounts of surface dust and the sampling location is often ill-defined. To remedy this situation, a sampling device which covers the entire bath depth was constructed. The equipment is shown in Fig. 1, and consists of a steel holder with a cup-shaped bottom and a quartz tube sample holder at the end of an aluminum tube. The bottom of the cup was covered with alumina before the device was introduced into the bath, then the quartz tube was slowly raised and subsequently lowered while immersed in the melt. After quenching in air, the sample was easily pushed out of the quartz tube and sliced into 20 mm high disks.

2.2. Oxidation analysis

The carbon content in the slices was determined by gravimetric oxidation analyses. The sample was heated by a vertical Kanthal wound tube furnace (16) controlled by a digital PID-regulator (Microcor II, Coreci). The temperature was recorded and controlled via a Pt/Pt10%Rh thermocouple. The experimental set-up is schematically presented in Fig. 2. The crucibles used for combustion analyses (reaction with O_2) were made of pure platinum. To eliminate problems due to wetting of platinum by cryolite melts, the gas inlet tube was made of an

95%Pt/5%Au alloy.

The samples (15g) were dried at 100 $^\circ$C and trans-
ferred to the crucible. The furnace with the sample
was evacuated and N2 (Norgas,99.9%) was admitted
during heating to the reaction temperature, 980 $^\circ$C.
Nitrogen was used as a carrier gas during the
oxidation, a 90%N_2/10%O_2 gas mixture was bubbled
through the melt. The gas mixture was led through
Dehydrite (Magnesium perchlorate, Merck, p.a.) and
Ascarite (Natronasbest 0.75-1.55 mm, Merck p.a.)
before entering the molten sample. To ensure
complete removal of HF from the exit gas from the
furnace, the gas mixture was led through NaF
(Merck, p.a.) at 0 $^\circ$C, NaF at 105 $^\circ$C and then
through a thorium nitrate - chrome azurole (Koch-
Light, pure) - H_2O indicator solution, which at
minute concentrations of fluorine changes color
from blue to light red. Moisture was removed from
the exit gas by contact with the magnesium perchlo-
rate. Carbon dioxide was collected in a tube 2/3
filled with Ascarite and 1/3 Dehydrite.

2.3 Microscopy

The samples were studied by optical microscopy in
order to determine the size distribution of the
dust particles as function of the bath depth. The
sliced disks were ground and dried, and finally
embedded in epoxy resin under vacuum. The surfaces
were then polished.

Analyses of the particle size distribution were
performed at SINTEF-NTH using a Leitz Texture
Analysing System. The total magnification was x80
and each investigated field was 0.465 mm wide. Per
sample, 30 fields were analysed, giving a resolu-
tion of 0.9 μm. At x344 magnification and 0.2 μm
resolution the contrast was too low for reliable
analysis.

Image analysis was also carried out at ASV's Metal
Research Laboratory. Eight images were made from
each sample using polarized light and x500 magnifi-
cation with a semi automatic Kontron-IBAS unit to
derive the particle size distribution.

3. RESULTS AND DISCUSSION

3.1 Image analyses

Results obtained using the Leitz TAS are shown for
several parallel samples in Table 1.

Table 1. Particle size distribution in samples
from prebaked and Soderberg cells at
normal operating conditions.

Cell type	Sample	Total %Area C	%Area C<4 μm	%Area C<15 μm	%Area C<40 μm
Prebaked	1	0.1	36	70	100
E-27	2	0.3	28	68	92
	3	0.5	24	63	91
	4	1.7	8	24	45
Average		0.7	24	56	82
Prebaked	1	0.02	50	100	100
	2	0.03	50	100	100
H-26	3	0.2	25	69	94
Average		0.08	45	90	98
Soder-berg	1	0.2	40	73	100
P-29	2	0.6	12	40	82
Average		0.4	26	57	91

The results show that the major particle size is
less than 15 μm and that practically all dust
particles are less than 40 μm. The exception is
E-27, which has only 45 % of the dust particles
smaller than 40 μm. This is probably due to a
certain content of larger coke grains in the
sample. As expected, the Soderberg cell is at a
higher dust level than the prebaked cells.
Although only two samples are investigated, the
size distribution seems to be shifted towards a
slightly higher content of coarser particles for
the Soderberg than observed for the prebaked
cells.

The statistical uncertainty in these measurements
will depend on the total carbon content, but will
be in the range +/- 3%. The uncertainty due to
uneven distribution of the dust particles will
probably be larger than the statistical, as indi-
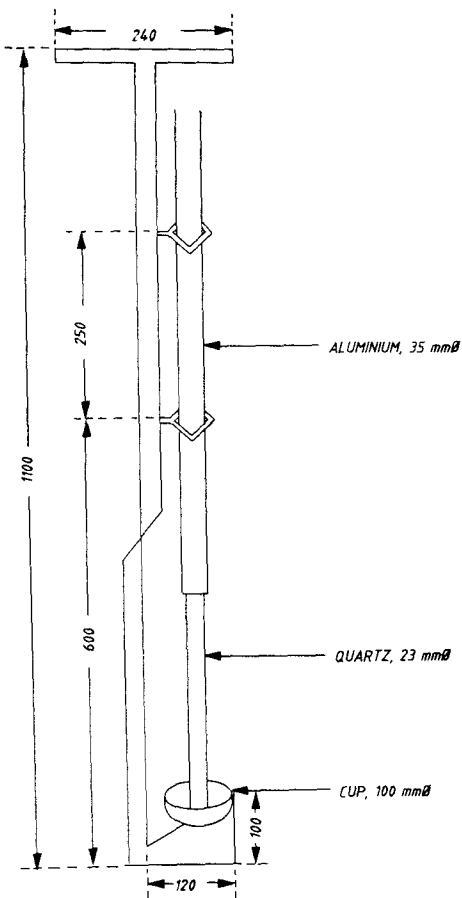cated in Table 1. Samples with a high dust content

Fig. 1 Equipment for sampling in aluminum reduction pots.

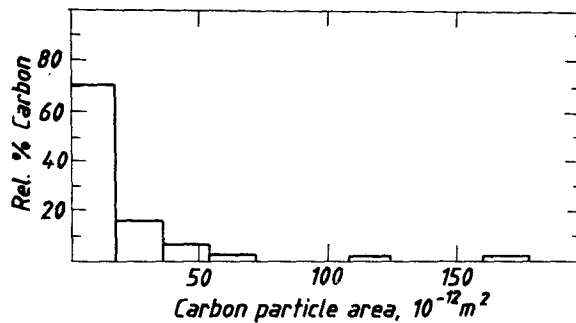Fig. 2. Experimental arrangement used for oxidation analyses.

Fig. 3 Dust particle size distribution in pot E14, sample 1 (prebaked).
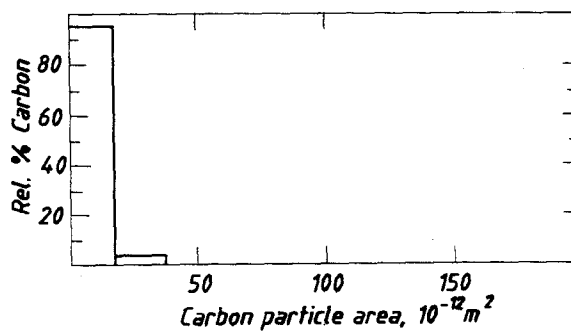
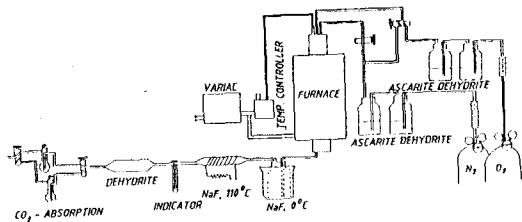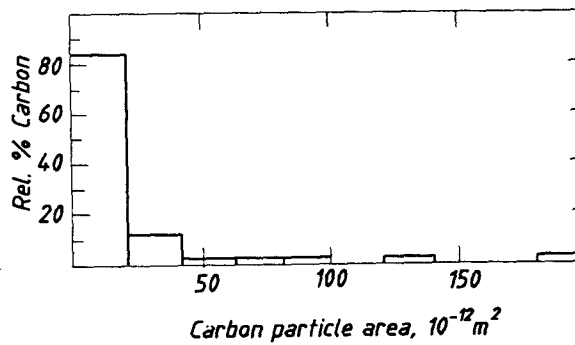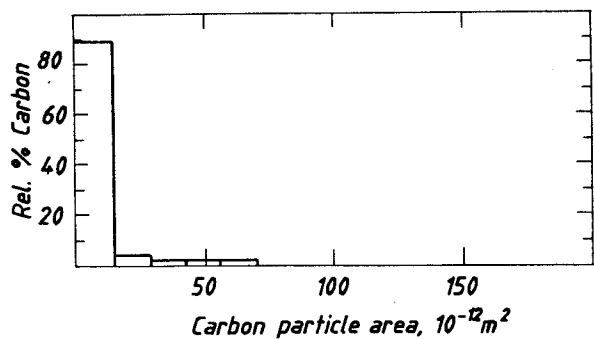Fig. 4 Dust particle size distribution in pot E14, sample 2 (prebaked).

Fig. 5 Dust particle size distribution in pot E14, sample 3 (prebaked).

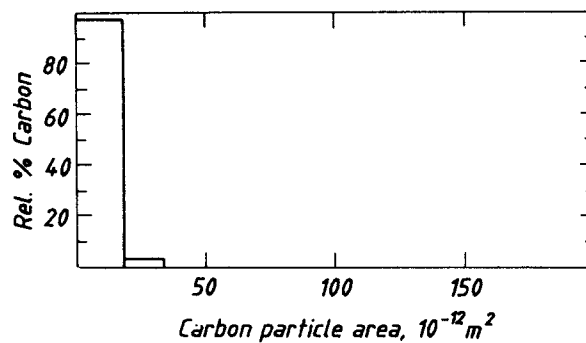Fig. 6. Dust particle size distribution in pot E14, sample 4 (prebaked).

Fig. 9. Dust particle size distribution in pot E14, sample 7 (prebaked).
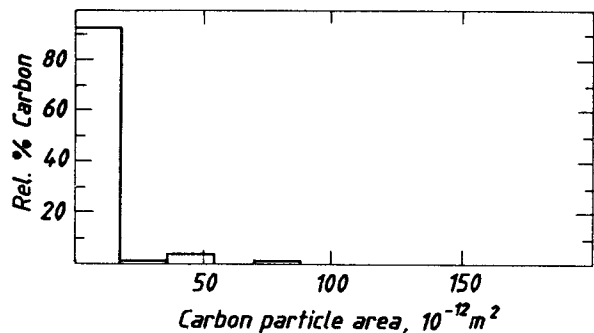

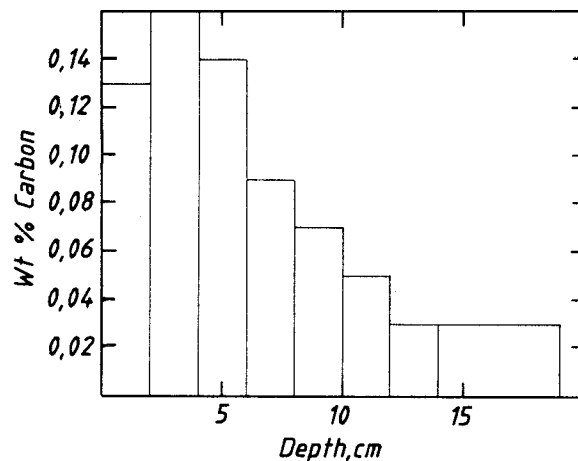Fig. 7. Dust particle size distribution in pot E14, sample 5 (prebaked).

Fig. 10. Dust content vs. bath depth, pot R27A (Soderberg).
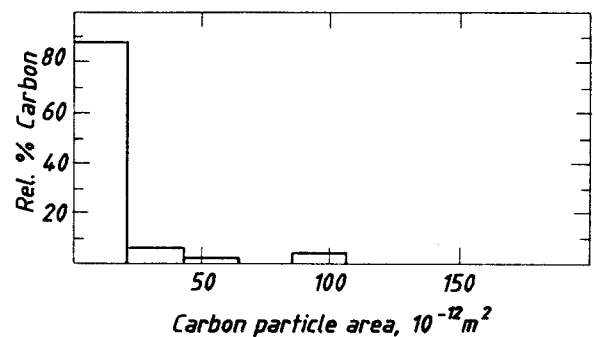

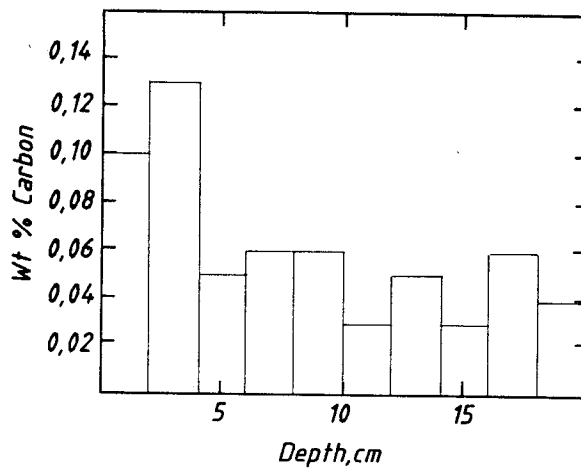Fig. 8. Dust particle size distribution in pot E14, sample 6 (prebaked).

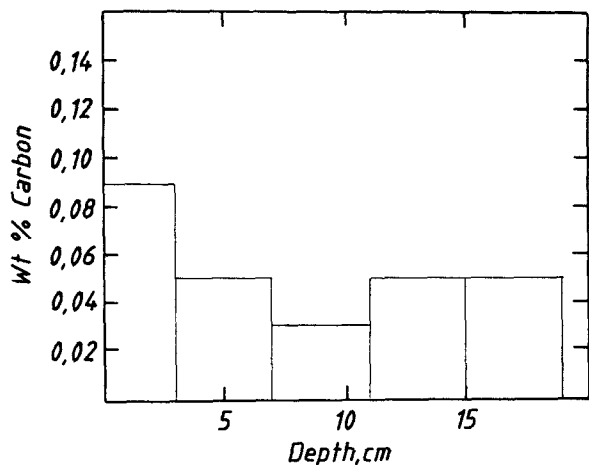Fig. 11. Dust content vs. bath depth, pot R24A (Soderberg).

Fig. 12. Dust content vs. bath depth, pot K40A (prebaked.)
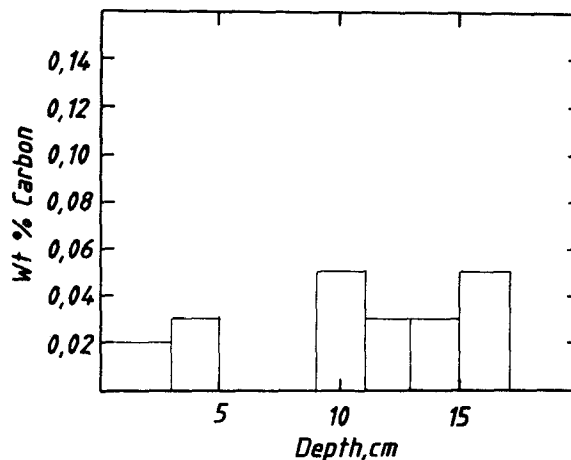

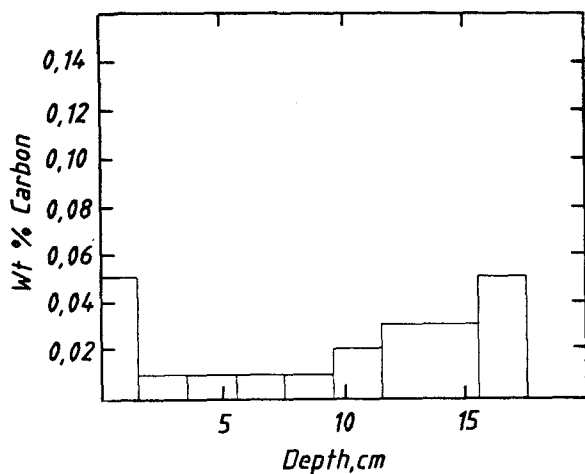Fig. 15. Dust content vs. bath depth, pot B30H (prebaked).

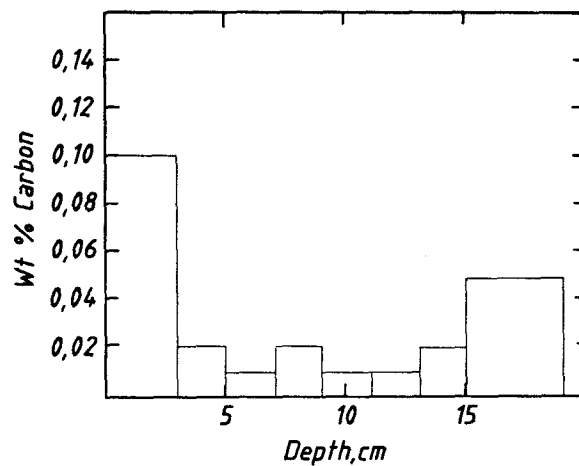

Fig. 13. Dust content vs. bath depth, pot E18A (prebaked).

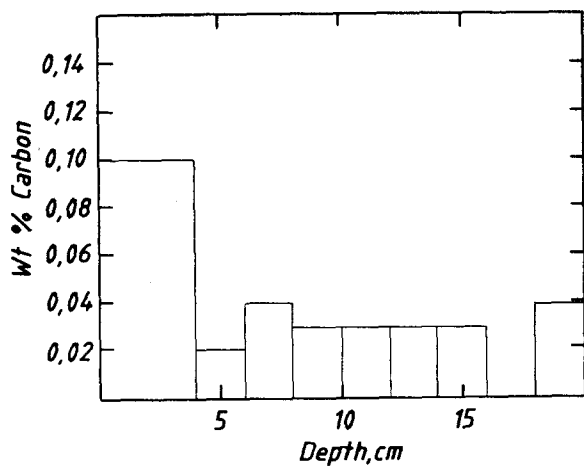Fig. 16. Dust content vs. bath depth, pot B26H (prebaked).

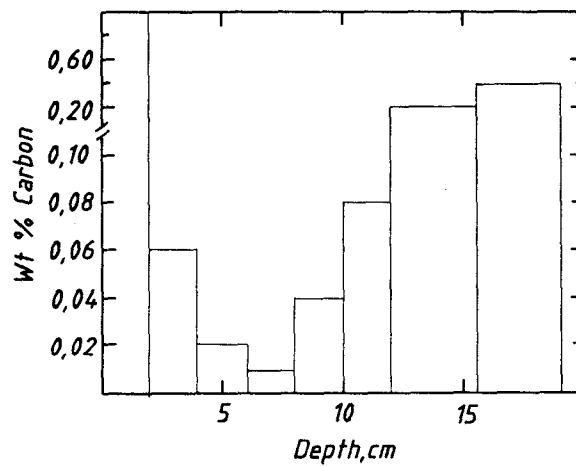Fig. 14. Dust content vs. bath depth, pot B31H (prebaked).

Fig. 17. Dust content vs. bath depth, pot A22H (prebaked.)

contain a smaller amount of fine particles than samples with a low dust level, indicating a content of coke grains.

The particle size distributions from the Kontron - IBAS analyses are given for a cell with prebaked anodes in Figs. 3-9 as the relative percentage of carbon in the sample versus dust particle area. Fig. 3 covers the region 0-20 mm, Fig. 4 20-40 mm, Fig. 5 40-60 mm, etc. in 20 mm regions, above the metal pad. The results show that 80-100 % of the dust particles have areas of less than 20 μm^2. The samples in Figs. 3 and 5, which are collected close to the metal and at the wearing surface of the anode, have 70 and 82 % of the particles in this size region, respectively. In addition, these are the only samples which contain particles with areas up to 200 μm^2, which may indicate that the largest dust particles are brought to the metal pad by frozen electrolyte (sludge), and that a size reduction mechanism is in operation for dust in the bulk electrolyte. The uncertainty using this method is calculated to be +/- 5 %, however, the error due to uneven carbon distribution in the sample may be even larger. With the magnification used, only 0.3 mm^2 of the sample surface is examined. If the uncertainty approaches 10 %, it will be larger than the difference between the different samples. The stirring introduced in the bath during sampling is considered to be negligible compared to the existing bath movement. However, slight freezing of the electrolyte on the quartz tube wall during tube lowering may have introduced an error in the carbon distribution around the tube periphery. Although this was not observed, microscopic studies were performed only at central parts of the disks.

3.2 Oxidation analysis

The total carbon content was measured versus the bath depth for 8 pots. The results are shown in Figs. 10 - 17. Although the results show a large degree of scatter, the dust is seen to be enriched close to the bath surface as well as at the metal - bath interface. Furthermore, in spite of analytical uncertainties, the results show that the dust level in Soderberg (0.07%) is the double compared to prebaked pots (0.04%).

The largest single error in the oxidation analyses is that Ascarite also reacts with other gas components than CO_2, and that small amounts of CO_2 is dissolved in the indicator solution (17). Blind tests established the maximum error in these analyses to be 13 %.

3.3. Density relations

The density of liquid electrolyte in the Hall - Heroult process is about 2.05 g/cm^3. Typical density values for calcined petrol coke are in the range 1.92 - 2.08 g/cm^3, whereas the density of the anode is 1.45 - 1.60 g/cm^3 (4). A graphite single crystal has a density of 2.25 g/cm^3 (18). The pore size distribution in carbon particles was measured (Carlo Erba 200 mercury porosimeter) in order to investigate the possibility that bath penetrates the pores of the particles to give increased density. The result of these measurements showed that more than 80 % of the pores have diameters smaller than 70 μm. It can be shown by calculations that the minimum pore radius for bath penetration will be in the range 90 - 150 μm. Hence, bath penetration will not greatly affect the density of the dust particles. Thus, by the single influence of gravity the dust partly will float on the bath surface and partly sink to the metal pad, in accordance with the observations in Section 3.2.

3.4 Possible reactions for carbon dust in the electrolyte

At high temperature aluminum and carbon may react to form aluminum carbide,

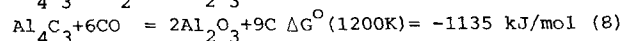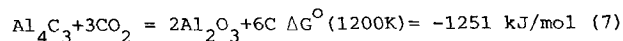$$4Al + 3C = Al_4C_3 \qquad (6)$$
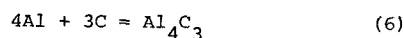
The reaction is thermodynamically favored at normal operating temperatures. Cryolite dissolves aluminum oxide and wets both the metal and the carbon. Thus, aluminum carbide can readily be formed and dissolved at aluminum - carbon - cryolite interfaces (19,20). The solubility of aluminum in the electrolyte is approximately 0.1 wt% (22 - 25). Dust particles at the metal-melt
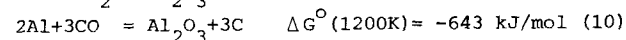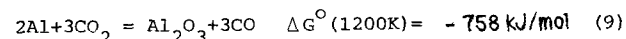
interface and in the bath then probably play an important role in aluminum carbide formation. Aluminum carbide is stable at alumina concentrations below 4 wt% and at higher concentrations as aluminum oxycarbide, Al_2OC (21).

The solubility of CO_2 in cryolite melts saturated with alumina at usual operating temperatures is about 0.01 wt% (29-32). The solubility of Al_4C_3 in the bath is 0.36 wt% at 1020 ^{o}C (26). It is hence conceivable that aluminum carbide formation, besides direct CO_2 - oxidation in the bath and air - oxidation at the bath surface may be the major reasons for the observed particle size distribution. Each of the investigated samples in this work showed the clear yellow color of Al_4C_3 at the metal - bath interface. Although the solubility of aluminum carbide in liquid aluminum is low (0.03 wt% at 950 ^{o}C) (27,28), its presence has negative effects on the rolling and pressing properties of the metal.
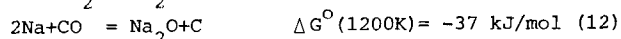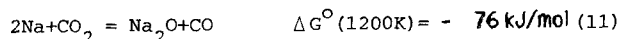
Aluminum carbide may be oxidized in the bath according to the following reactions:

$$Al_4C_3+3CO_2 = 2Al_2O_3+6C \quad \Delta G^{o}(1200K)= -1251 \text{ kJ/mol} \quad (7)$$
$$Al_4C_3+6CO = 2Al_2O_3+9C \quad \Delta G^{o}(1200K)= -1135 \text{ kJ/mol} \quad (8)$$

Reactions (7) and (8) are thermodynamically strongly favored (33) and the carbon released will be in the form of very small particles. Another reaction scheme to give fine carbon particles will be (33):

$$2Al+3CO_2 = Al_2O_3+3CO \quad \Delta G^{o}(1200K)= -758 \text{ kJ/mol} \quad (9)$$
$$2Al+3CO = Al_2O_3+3C \quad \Delta G^{o}(1200K)= -643 \text{ kJ/mol} \quad (10)$$

It has been shown (34) that part of the CO_2 formed during electrolysis is consumed by back reaction with dissolved metal under formation of CO and that a small amount of the produced CO can react to form carbon. Carbon monoxide also can be produced in the melt by reaction between C and CO_2 or O_2 (Eqns. (3) and (5)). Sodium formed during the electrolysis makes an additional mechanism conceivable (33):

$$2Na+CO_2 = Na_2O+CO \quad \Delta G^{o}(1200K)= -76 \text{ kJ/mol} \quad (11)$$
$$2Na+CO = Na_2O+C \quad \Delta G^{o}(1200K)= -37 \text{ kJ/mol} \quad (12)$$

Thus, various reaction schemes may contribute as

possible particles size reducing mechanisms to produce the relatively large amounts of fine dust particles which occur in Hall - Heroult cells. Although in general the direct oxidation by O_2 at the bath surface and reaction with dissolved CO_2 in the bath are expected to be the main reasons for carbon dust for formation, the other mechanisms are likely to co - exist.

3.5 Operational effects

The accumulated dust in the inter electrode space effectively reduces the area available for current passage and increases the bath resistance. It is possible to calculate the increase in cell resistance as function of the dust content if the dust particles are assumed to be spherical and randomly distributed in the bath. If the pure bath interpolar resistance is R, the fractional change in the cell resistance is expressed by:

$$\Delta R/R \approx A_c/(A_b - A_c) \quad (13)$$

where A_c is the total area covered by the dust particles and A_b is the total conducting area of a pure electrolyte pot. Table 2 shows the relation between the dust content in the electrolyte and the increase in the interpolar resistance as calculated from Eqn.(13).

Table 2. Relation between the concentration of dust particles in the electrolyte and the increase in bath resistance.

Wt%C	0.01	0.05	0.1	0.5	1.0
$\Delta R/R$(%)	0.3	0.8	1.2	3.7	6.0

Although this calculation is simplified, it demonstrates the fact that relatively small amounts of dust may cause a considerable increase in the cell resistance. As mentioned earlier this, combined with carbon dust burning at the electrolyte's surface, causes an increase in the bath temperature and accelerates the dusting problem. It has been argued (13) that if less than 10 % of

the anodes of a cell have inferior dusting charc-
teristics, the total amount of dust in the cell
will be small and not cause operational problems.
However, with 15 - 20 % anodes of high dusting
ability the operational situation quickly deter-
iorates and increases the anode consumption.

The dust concentration represents the balance
between the dust formation and dust consumption
rates. Thus, the accumulated level may be signifi-
cantly influenced by the cell design, operation and
practice including crust breaking and ore/bath
covering procedure. In a limited number bench scale
experiments air was injected into melts containing
0.1 wt% carbon, and approximately 40 % of the
carbon was removed within 15 min bubbling, indi-
cating a way to control the dust level in aluminum
reduction pots. Besides representing an excessive
specific carbon consumption, dusting may cause
losses in current efficiency through direct current
leaks as well as through side reactions with
dissolved aluminum. The major basic exercise to
avoid carbon dusting is to balance the reactivities
of the various anode phases towards O_2 and CO_2.

References

1. K. Grjotheim, C. Krohn, M. Malinovsky, K. Matia-
   sovsky and J. Thonstad, "Aluminium Electolysis -
   Fundamentals of the Hall-Heroult Process",
   Aluminium Verlag, Dusseldorf, 1982, p.391.

2. R. Farr-Wharton, B.J. Welch, R.C. Hannah, R.
   Dorin and H.J. Gardner, Electrohim. Acta 25
   (1980)217.

3. S.S. Jones and R.D. Hildebrandt, Light Metals
   1974, p.901.

4. K. Grjotheim and B.J. Welch, "Aluminium Smelter
   Technology - A Pure and Applied Approach",
   Aluminium Verlag, Dusseldorf, 1980.

5. E.A. Hollingshead and V.A. Braunwarth, in
   "Extractive Metallurgy of Aluminium", G. Gerad,
   ed., Interscience Publishers, New York, Vol.2,
   1962, p.31.

6. P.J. Barat, T. Brault and J.P. Saget, Light
   Metals 1974, p.19.

7. P.J. Rhedey, Light Metals 1982, p.713.

8. P.J. Rhedey, Light Metals 1971, p.385.

9. R.R. Adair, E.H. Boult, E.M. Freeman, S.
   Jasienko and H. March, Carbon 9(1971)763.

10. E.T. Turkdogan and J.V. Vinters, Tenth Bien.
    Conf. Carbon, RS 158(1971)294.

11. G.J. Houston and H.A. Øye, Aluminium 61(1985)
    251.

12. R. Farr-Wharton, Ph.D. Thesis, The University
    of New South Wales, Australia, 1980.

13. E. Barillon, "Mechanism of Carbon Dust Forma-
    tion in Aluminium Electrolysis", Milan, Italy,
    1971.

14. B.P. Domrachev and M.A. Korobov, Tsvet. Met.
    44(1971)30.

15. J.F. Rey Boero, Light Metals 1981, Proceedings
    of Sessions, 110th AIME Annual Meeting,
    Chicago, Illinois, 1981, p.44.

16. K. Motzfeldt, in "Physicochemical Measurements
    at High Temperature", J.O'M. Bockris, J.L.
    White and J.D. Mackenzie, eds., Butterworths
    Scientific Publications, London 1959, p.51.

17. G.H. Aylward and T.J.V. Findlay, "SI Chemical
    Data", Wiley, Sydney, 1971.

18. C.L. Mantell, "Carbon and Graphite Handbook",
    1.ed., Interscience Publishers, New York,
    1968.

19. R.C. Dorward, Light Metals 1973, p.105.

20. K. Grjotheim, R. Næumann, and H.A. Øye, Light
    Metals 1977, p.233.

21. K. Grjotheim, O. Herstad, R. Næumann and H.A.
    Øye, Light Metals 1978, Vol.1, p.107.

22. H. Kvande, Light Metals 1980, p. 171.

23. J. Thonstad, Can.J.Chem., 43(1965)3429.

24. S. Rolseth and J. Thonstad, Light Metals 1981,
    p.289.

25. W.E. Haupin, J. Electrochem.Soc., 107(1960)232.

26. J.A. Brown and E.A. Hollingshead, Paper
    presented at the 97th AIME Annual Meeting, New
    York, 1968.

27. P.T. Stroup, Trans.Met. Soc.AIME 230(1964)356.

28. H. Ginsberg and V. Sparwald, Aluminium
    41(1965)181.

29. D. Bratland and C. Krohn, Tidsskr. Kjemi,
    Bergv., Metallurgi 26(1966)81.

30. D. Bratland, K. Grjotheim, C. Krohn and K.
    Motzfeldt, J. Metals 19(1967)13.

31. D. Bratland, Dissertation, Institute of
    Inorganic Chemistry, The University of
    Trondheim, Norway 1966.

32. H. Numata and J.O'M. Bockris, Light Metals
    1984, 759.

33. JANAF Thermochemical Tables, 2nd ed., NSRDS –
    NBS 37, US Dept. of Commerce, Washington DC
    1971.

34. J. Thonstad and A. Solbu, Trans. Met. Soc. AIME
    242(1968)301.